CrossMark

RESEARCH PAPER

Generalized green synthesis of Fe$_3$O$_4$/Ag composites with excellent SERS activity and their application in fungicide detection

Hongyan Guo · Aiwu Zhao · Rujing Wang · Dapeng Wang · Liusan Wang · Qian Gao · Henghui Sun · Lei Li · Qinye He

Abstract This paper reports the generalized green synthesis of a series of Fe$_3$O$_4$/Ag composites by magnetron sputtering method. The amounts of silver nanoparticles located on the hollow Fe$_3$O$_4$ magnetic nanoparticles can be tuned by controlling the sputtering time. The surfaces of Fe$_3$O$_4$/Ag composites are rough with high density and numerous Ag nanogaps (which can serve as Raman active hot spots to amplify the Raman signal), providing the sound reliability and reproducibility of Raman detection. With p-aminothiophenol and Rhodamine 6G (R6G) for probe molecules, the surface-enhanced Raman scattering (SERS) properties of these Fe$_3$O$_4$/Ag composites were studied. It was found that the SERS signal reached the maximum with the sputtering time of 130 s, indicating that this compound had most hot spots. In this paper, we used the composite with the strongest SERS signal for thiram detection, and the detection limit can reach 5×10^{-7} mol/L (about 0.012 ppm), which is lower than the maximal residue limit of 7 ppm in fruit prescribed by the U.S. Environmental Protection Agency. The Fe$_3$O$_4$/Ag composites are readily available, easy to carry, and show great potential for applications in universal SERS substrates in practical SERS detection.

Keywords Fe$_3$O$_4$/Ag composites · Surface-enhanced Raman scattering · p-aminothiophenol · Rhodamine 6G · Thiram detection · Sensors

H. Guo · A. Zhao · D. Wang · L. Li · Q. He
Department of Chemistry, University of Science and Technology of China, Hefei 230026, Anhui, People's Republic of China

H. Guo · A. Zhao (✉) · R. Wang · D. Wang · L. Wang · Q. Gao · H. Sun · L. Li · Q. He
Institute of Intelligent Machines, Chinese Academy of Sciences, Hefei 230031, People's Republic of China
e-mail: awzhao@iim.ac.cn

H. Guo · A. Zhao · D. Wang · Q. Gao · H. Sun
State Key Laboratory of Transducer Technology, Chinese Academy of Sciences, Hefei 230031, People's Republic of China

Introduction

In recent years, surface-enhanced Raman scattering (SERS) has been a powerful and versatile novel analytical tool due to its high sensitivity and specificity in the detection of analytes (Lal et al. 2008; Lee et al. 2010; Xia et al. 2011; Su et al. 2012). Thus, the SERS technology has been widely applied in biology, medicine pharmacy, environmental monitoring, national security, and other fields (Zong et al. 2012; Yang et al. 2014; Tao et al. 2014; Wang et al. 2014). Typically, probe molecules adsorbed on the surface of noble metals (Ag, Au, or Cu) and some transition metals can produce significant SERS effect. Theoretically, the size and shape can affect their SERS properties (Guo et al. 2009). Therefore, various shapes of these nanoparticles (NPs) with different size have

been prepared and their SERS properties have been greatly investigated, such as nanospheres, nanorods, nanowires, nanocubes, nanocages, core/shell structures, and so on (Guo et al. 2009; Njoki et al. 2007; Orendorff et al. 2005; Liu et al. 2013; Skrabalak et al. 2007; Chen et al. 2007; Panda et al. 2007; Bao et al. 2008). Although they have excellent SERS properties, there are some limitations in the application. The noble metals not only directly increase the cost of the SERS application, but also tend to aggregate, and it is troublesome to be separated and concentrated. To resolve these problems, the magnetic nanoparticles were introduced. They can be easily separated and concentrated by applying an external magnetite (Mariotti and Sankaran 2010). They usually combine with noble metal to form magnetic/noble metal composites as SERS substrates (Gühlke et al. 2012; Lv et al. 2010; Tian et al. 2012; Yang et al. 2012).

Magnetic/noble metal composites have attracted particular attention, due to the combined functions of magnetic and optical properties from the two components. Therefore, the multifunctionality makes the composites to be widely applied in catalysis, targeted drug delivery, magnetic resonance imaging, and SERS detection (Zhang et al. 2010; Xuan et al. 2011; Xu et al. 2009; Gao et al. 2011, 2012; Gan et al. 2013; Guo et al. 2014). Currently, there are two methods for preparing magnetic/noble metal composites, namely one-step and multi-step processes. Gong and his colleagues reported a one-step method to synthesize rattle-type $Pd@Fe_3O_4$, $Ag@Fe_3O_4$, and $Cu@Cu_{x-}Fe_{3-x}O_4$ composites (Jiang et al. 2012). They pointed out that these complexes had high catalytic activity. Zhang has prepared $Ag@Fe_3O_4$ core/shell nanostructures and studied their plasmonic and catalytic properties (Zhang et al. 2012; Sun et al. 2013). They modulated the size and morphology of the nanostructures by controlling the reaction time and the molar ratio of Ag/Fe precursors. They also proved that the $Ag@Fe_3O_4$ nanostructures were recyclable catalysts in the reduction of R6G. There were many other reports about one-step preparation of noble metal/magnetic composites, but mostly studied their catalytic properties. Fe_3O_4/noble metal composites are generally prepared using a multi-step method. Fe_3O_4 nanoparticles were firstly synthesized by the solvothermal approach, and then the surface was modified with the link molecule. With the linker, the noble metal was finally contacted on the surface of

Fe_3O_4 nanoparticles to form the composites. Wang's group constructed multifunctional Fe_3O_4/metal hybrid nanostructures using 3-aminopropyltrimethoxysilane (APTMS) as a linker (Guo et al. 2009). Au NPs, Au/Pt hybrid NPs, and Au/Ag core/shell NPs were supported on the surface of Fe_3O_4 spheres. These multifunctional hybrid spheres showed high catalytic activity. Since the surface of Fe_3O_4 was coated with high-density Ag or Au/Ag core/shell NPs, they showed good SERS activities. Bao acquired γ-Fe_2O_3/Au core/shell NPs by deposition of Au on the preformed Fe_2O_3 using iterative hydroxylamine seeding procedure (Bao et al. 2009). The SERS properties of the products were studied and applied in immunoassay. In addition, there are some reports about the noble metal coated on the magnetic material surface through electrostatic adsorption. Dong reported a multi-step method to synthesize Fe_3O_4/Au submicrometer structures (Zhai et al. 2009). The Fe_3O_4 particles were first modified with polyelectrolytes to impart positive charge and then electrostatically adsorbed a lot of gold nanoseeds for further Au shell formation. Au shells were finally formed by reduction of $HAuCl_4$ with hydroxylamine. Tang designed Au nanorod-coated Fe_3O_4 microspheres for near-infrared SERS application (Tang et al. 2015). In this report, the Fe_3O_4 microspheres were synthesized by hydrothermal method, surface functionalized with polyethylenimine, and then coated with Au nanorods densely. To meet the different needs of the application, Fe_3O_4@C@Au, Fe_3O_4@SiO_2@-Ag, Fe_3O_4@SiO_2@Au, Au@Fe_3O_4@SiO_2, Ag@Fe_3-O_4-SiO_2 Janus nanorod, and other multifunctional composites were prepared (Qi et al. 2010; Jun et al. 2011; Khosroshahi and Ghazanfari 2012; Bardhan et al. 2009; Zhang et al. 2012). Since magnetic/noble metal composites comprise noble metal outside, their SERS properties and SERS-based applications were greatly investigated in previous studies. However, the stability of SERS substrate and the reproducibility of the signal have always been the problem to be resolved.

In this paper, we report a stable and efficient route based on physical magnetron sputtering technique for preparing Fe_3O_4/Ag composites with high SERS activity. The surface morphology of these composites was reproducible where strong SERS signals can be generated. Both the SERS signal of p-aminothiophenol (PATP) and R6G reached the maximum with a sputtering time of 130 s. These composites were also

applied for the detection of thiram and the detection limit was as low as 5×10^{-7} M (about 0.012 ppm). It is noted that the obtained Fe_3O_4/Ag composites are stable and can be produced on a large scale with high repeatability. Moreover, the formed silicon slide SERS substrates are easy to carry and can be cut into pieces for direct detection, which show great potential for the rapid ultratrace detection of contaminants in soil and water.

Experimental section

Chemicals and materials

Ferric nitrate nonahydrate ($Fe(NO_3)_3 \cdot 9H_2O$), sodium citrate, urea, polyacrylamide (PAM), silver nitrate ($AgNO_3$), rhodamine 6G (R6G), and thiram were purchased from Shanghai Reagents Co (China). PATP was supplied by Alfa-Aesar. All of the chemical reagents were of analytical grade and used as received without further purification. All glasswares were cleaned with aqua regia, thoroughly rinsed with deionized water, and dried prior to use.

Synthesis of hollow Fe_3O_4 NPs

Hollow Fe_3O_4 NPs were synthesized by the solvothermal approach (Xuan et al. 2011). In the typical procedure, $Fe(NO_3)_3 \cdot 9H_2O$ (0.45 mmol) was dissolved in H_2O to form a clear solution, followed by the addition of sodium citrate (1.8 mmol), urea (1.8 mmol), and PAM (0.09 g). Deionized water was added to the mixture until the final volume to 12 mL. The mixture was stirred vigorously until all the reactants were fully dissolved. Then, the obtained solution was transferred to a 15-mL Teflon-lined stainless steel autoclave and heated at 200 °C for 12 h. The autoclave was allowed to cool down to room temperature naturally. Finally, the black precipitate was collected by the magnet and rinsed with water and ethanol, then dried under vacuum at 60 °C for subsequent experiments.

Preparation of Fe_3O_4/Ag composites

Fe_3O_4 NPs dispersed in ethanol was firstly concentrated onto the cleaned silicon slides under the external magnetic field. After dried with high purity nitrogen, the silicon substrate was placed in the conventional direct-current magnetron sputtering system to deposit Ag. The power of the magnetron was 50 W, the pressure of the magnetron chamber was 5×10^{-1} Pa, and the deposition time was, respectively, 40, 70, 100, 130, 160, and 190 s. The samples were conserved with nitrogen protection before further experiments. For SERS detection, each sample substrate was cut into pieces. These SERS substrates were immersed in PATP, R6G, and thiram ethanol solutions for 2 h. Then, the substrates were taken out, rinsed with ethanol, and dried with high-purity nitrogen before detection. Scheme 1 shows the formation of Fe_3O_4/Ag composites and the SERS detection process.

Characterization

The morphologies of the samples were observed with field emission scanning electron microscope images (FESEM) on a JEOL JSM-6300F SEM with primary electron energy of 10 kV. Transmission electron microscopy (TEM) studies were performed with a JEOL-2010 microscope operated at an accelerating voltage of 200 kV with a tungsten filament. The phase and composition of the products were determined by a Rigaku D/Max-γA rotating-anode X-ray diffractometer equipped with monochromatic high-intensity Cu-Kα radiation ($\lambda = 1.54187$ Å). The magnetic properties of the samples were measured by the Magnetic Property Measurement System (MPMS, XL5) at 300K. The Raman scattering spectra were recorded on Thermo Fisher DXR Raman Microscope equipped with a CCD detector in backscattered configuration using a $10\times$ objective, and the Raman spectra were recorded with a 532 nm laser, 1 mW power, 50 μm aperture slit, and 5 s integral time.

Results and discussion

Synthesis and characterization of Fe_3O_4/Ag composites

At the beginning of the experiment, an aqueous mixture of Fe (III) ions, sodium citrate, urea, and polyacrylamide (PAM) was prepared. After the hydrothermal treatment process, porous spherical type nanoparticles were obtained. The morphology of the obtained pure Fe_3O_4 NPs was characterized by SEM

**Scheme 1** The formation of Fe$_3$O$_4$/Ag composites and the SERS detection process
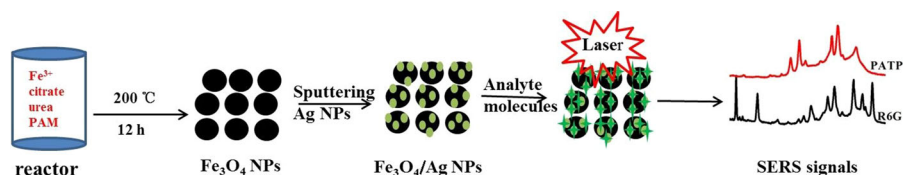
and TEM. As shown in Fig. 1A, there are uniformly porous spherical nanoparticles and the diameter is about 250 nm. From Fig. 1B, the surface of Fe$_3$O$_4$ NPs is relatively rough which indicate that the particle is composed of tiny primary nanocrystals. The phase structure of the obtained sample was characterized by XRD. From Fig. 1C, the XRD pattern of the obtained sample proves its crystalline nature and the peaks match well with standard Fe$_3$O$_4$ reflections (JCPDS card No. 88-0315). The magnetization of obtained pure Fe$_3$O$_4$ NPs will be studied later. Figure 1D shows the magnetic hysteresis loops of the sample, and the saturation magnetization is 112 emu/g. The

magnetization is strong enough that they can be easily concentrated and separated from the solution by simply applying a small magnet.

The morphology of the obtained composites with different amounts of Ag was characterized by SEM in Fig. 2. As can be seen from the figure, the amount of Ag is increasing as sputtering time increases. The amount of Ag reaches the maximum at 190 s and there is an obvious Ag layer on the next blank silicon wafer. Particularly, the surface of the composites with a sputtering time of 130 s is relatively rough compared with others. This rough structure may produce more hot spots in the subsequent SERS detection.

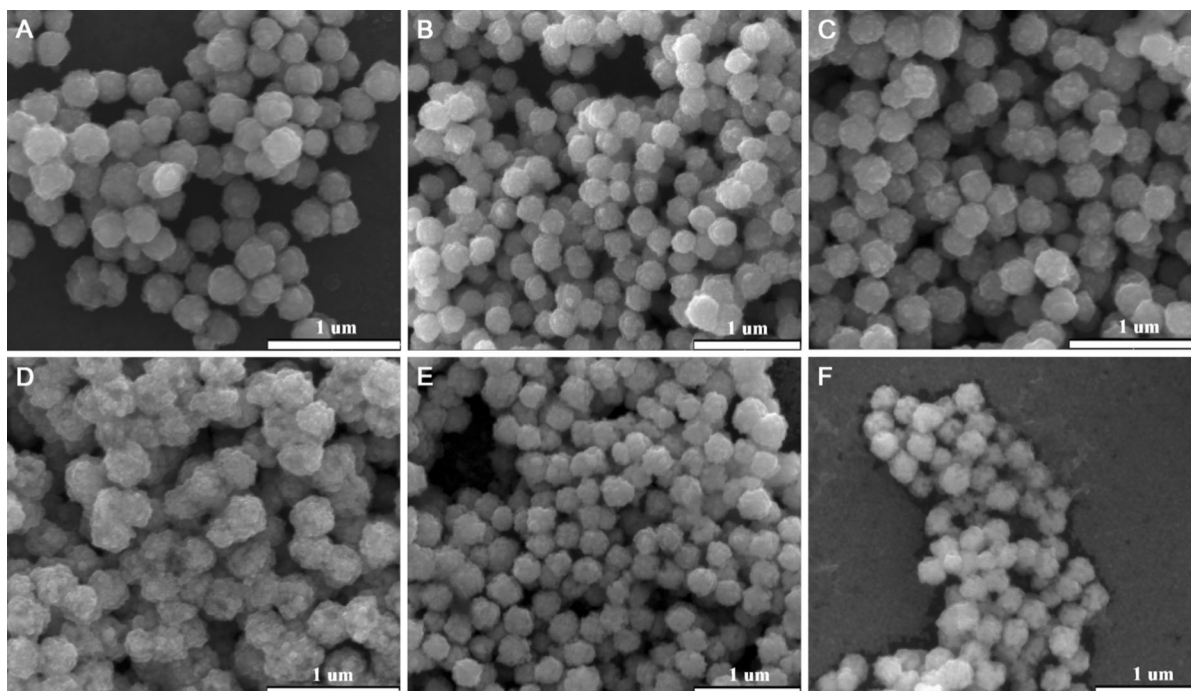**Fig. 1** The morphology and properties of the obtained Fe$_3$O$_4$ NPs: SEM (**A**), TEM (**B**), XRD (**C**), and *M–H* curve (**D**)
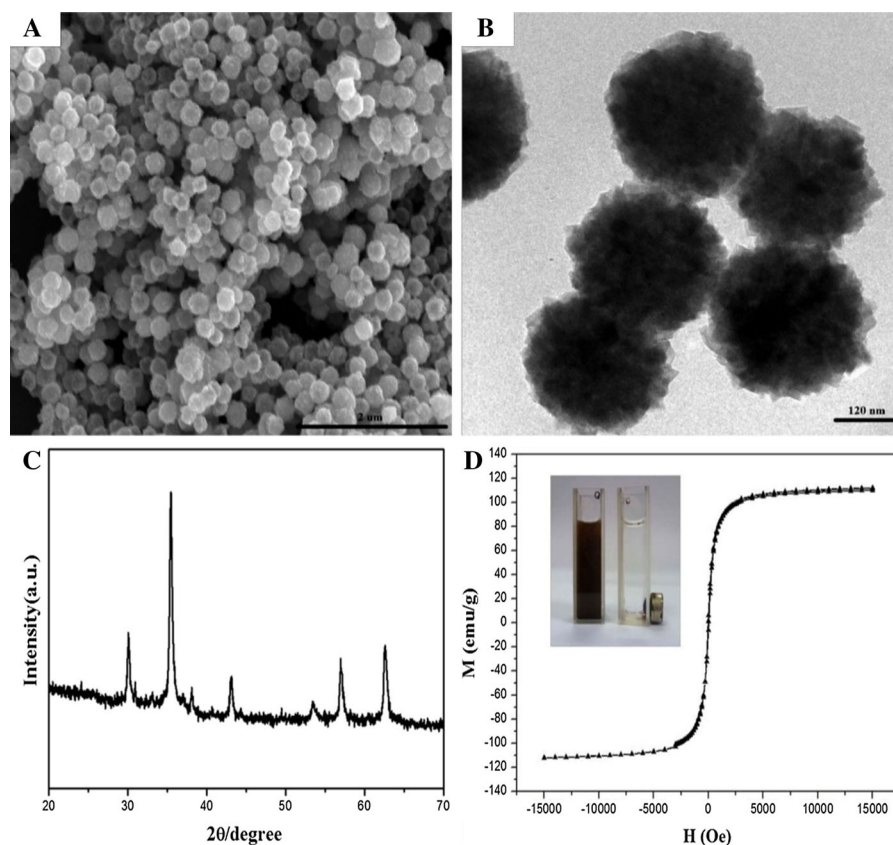
Fig. 2 SEM images of Fe_3O_4/Ag composites with a sputtering time of 40 (**A**), 70 (**B**), 100 (**C**), 130 (**D**), 160 (**E**), and 190 s (**F**)

SERS properties of the Fe_3O_4/Ag composites

The performance of the Fe_3O_4/Ag composites as SERS active substrates was initially investigated with PATP (1.0×10^{-5} M) and R6G (1.0×10^{-7} M) as the target analytes. The excitation power was 1.0 mW and the integration time was 5 s for each spectrum. Figure 3A shows the SERS spectra of PATP adsorbed on the Fe_3O_4/Ag composites with different sputtering time. Distinctive SERS spectra were obtained and the peak positions agreed well with the PATP molecules adsorbed on silver nanostructures (Osawa et al. 1994). Five strong bands at 1077, 1142, 1388, 1437, and 1577 cm^{-1} are attributed to the benzene ring in-plane and out-of-plane vibrations. It is observed that the SERS intensity increases with the extension of the sputtering time and reaches a maximum at 130 s, then decreases at 160 and 190 s (Zhang et al. 2014). Figure 3B presents the integrated SERS intensities of bands at 1142 and 1437 cm^{-1} observed in Fig. 3A as a function of sputtering time. It is clear that the sample showed the strongest SERS signal at the sputtering time of 130 s. At the beginning of 40 s, sparse silver NPs were decorated onto the surface of Fe_3O_4 NPs

which produced a minimum SERS signal. As the sputtering time prolongs, the number of silver NPs increases which tends to form a large number of gaps on the surface. These gaps may provide more active sites which afford potential hot spots to enhance the SERS signal (Rodríguez-Fernández et al. 2009). However, the formed gaps would be covered by silver NPs with further increasing sputtering time which reduces the potential hot spots, thus reducing the SERS intensity.

For further proving the correlation of SERS properties and Fe_3O_4/Ag composites with increasing sputtering time, R6G was chosen to repeat the experimental process. Figure 4A shows the SERS spectra of R6G adsorbed on the prepared samples. There are five strong SERS peaks appearing at 1187, 1311, 1362, 1509, and 1651 cm^{-1} which are assigned to C–H in-plane bending, C–O–C stretching, and C–C stretching of the aromatic ring (Sun et al. 2008). The peak at 772 cm^{-1} is due to the out-of-plane bending motion of the hydrogen atoms of the xanthene skeleton (Xu et al. 1999). Figure 4B presents the integrated SERS intensities of bands at 613 and 1362 cm^{-1} observed in Fig. 4A as a function of sputtering time.
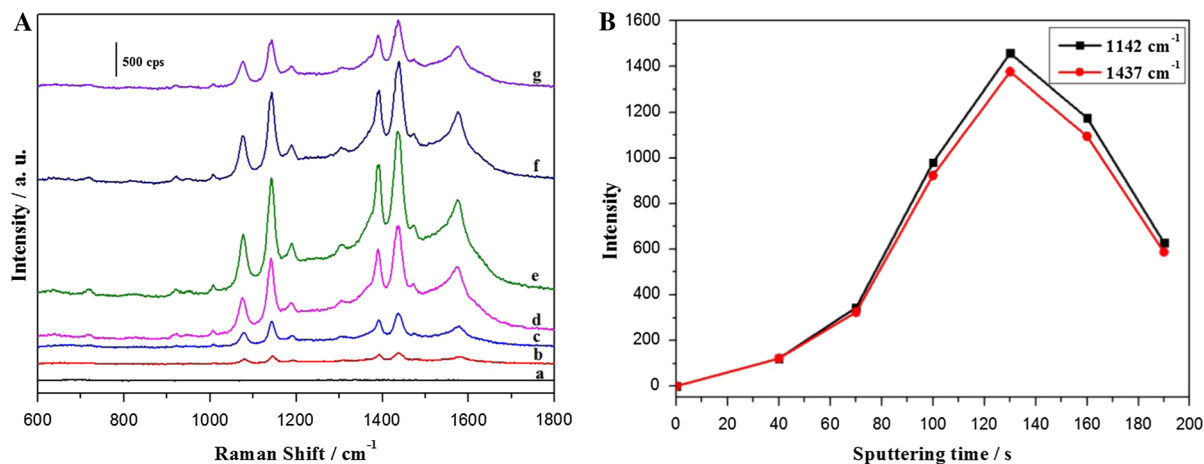
Fig. 3 A SERS spectra of PATP (10^{-5} M) adsorbed on the Fe$_3$O$_4$/Ag composites with the sputtering time of 0 (*a*), 40 (*b*), 70 (*c*), 100 (*d*), 130 (*e*), 160 (*f*), and 190 s (*g*). The excitation power was 1.0 mW and the integration time was 5 s. **B** The trend of peaks at 1142 and 1437 cm^{-1} of the PATP adsorbed on the composites with different sputtering time
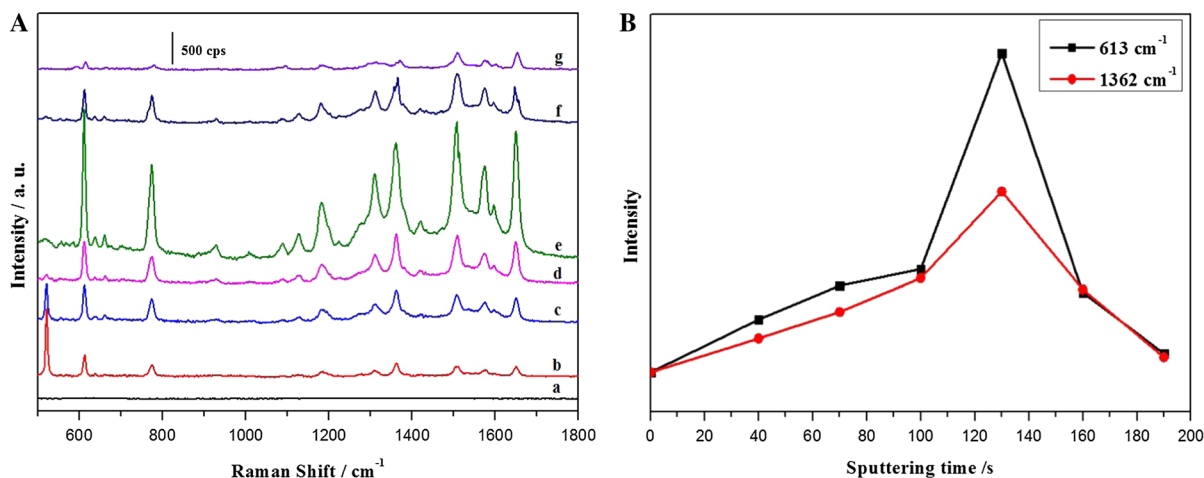

Fig. 4 A SERS spectra of R6G (10^{-7} M) adsorbed on the Fe$_3$O$_4$/Ag composites with the sputtering time of 0 (*a*), 40 (*b*), 70 (*c*), 100 (*d*), 130 (*e*), 160 (*f*), and 190 s (*g*). The excitation power was 1.0 mW and the integration time was 5 s. **B** The trend of peaks at 613 and 1362 cm^{-1} of the R6G adsorbed on the composites with different sputtering time

As can be seen, the SERS signal of R6G reached the maximum at 130 s, which agreed well with the variation tendency of PATP.

The above proves that the Fe$_3$O$_4$/Ag composites have excellent SERS performance. Then, the composite with a sputtering time of 130 s was chosen for detection sensitivity study. Figure 5 shows the SERS spectra of PATP with different concentrations adsorbed on the Fe$_3$O$_4$/Ag with a sputtering time of 130 s. The characteristic peaks of PATP are obvious. These results demonstrate that PATP adsorbed on the composite SERS substrate can be well detected in the

concentration ranges down to 1×10^{-10} M. While using SERS technology to detect target molecules in the practical application, the reproducibility and stability of Fe$_3$O$_4$/Ag SERS substrate must be validated. The SERS mapping is often used to estimate the reproducibility of SERS signals. In this paper, the area scanning mapping of the composite with a sputtering time of 130 s is shown in Fig. 6, which was based on the intensity of the spectral peak at 1142 and 1437 cm^{-1} of PATP. It can be seen that there is a homogeneous SERS response throughout the whole surface with a scale of 5 cm. Except for some
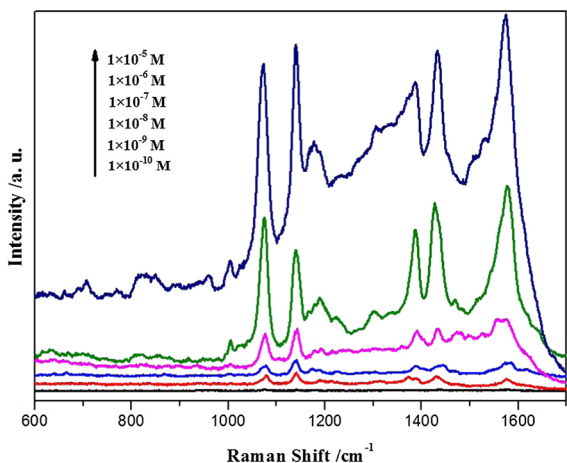
Fig. 5 Series of SERS spectra of PATP at different concentrations adsorbed on the Fe$_3$O$_4$/Ag composites with a sputtering time of 130 s

inevitable defect spots, data show that our Fe$_3$O$_4$/Ag composites are excellent SERS substrates. In addition, the Fe$_3$O$_4$/Ag substrates are stable and can be produced with high reproducibility across the entire area, which show great potential for application in pesticide detection.

SERS detection of thiram

The Fe$_3$O$_4$/Ag composites were further applied for the trace detection of thiram. The thiram is a low-toxicity fungicide which is widely used in plant insecticide. It has a stimulating effect on the skin and respiratory mucosa. There are many methods reported for the detection of thiram, such as chromatography, UV–Vis spectrophotometry, enzyme-linked immunosorbent assay, and chemiluminescence analysis (Gupta et al.
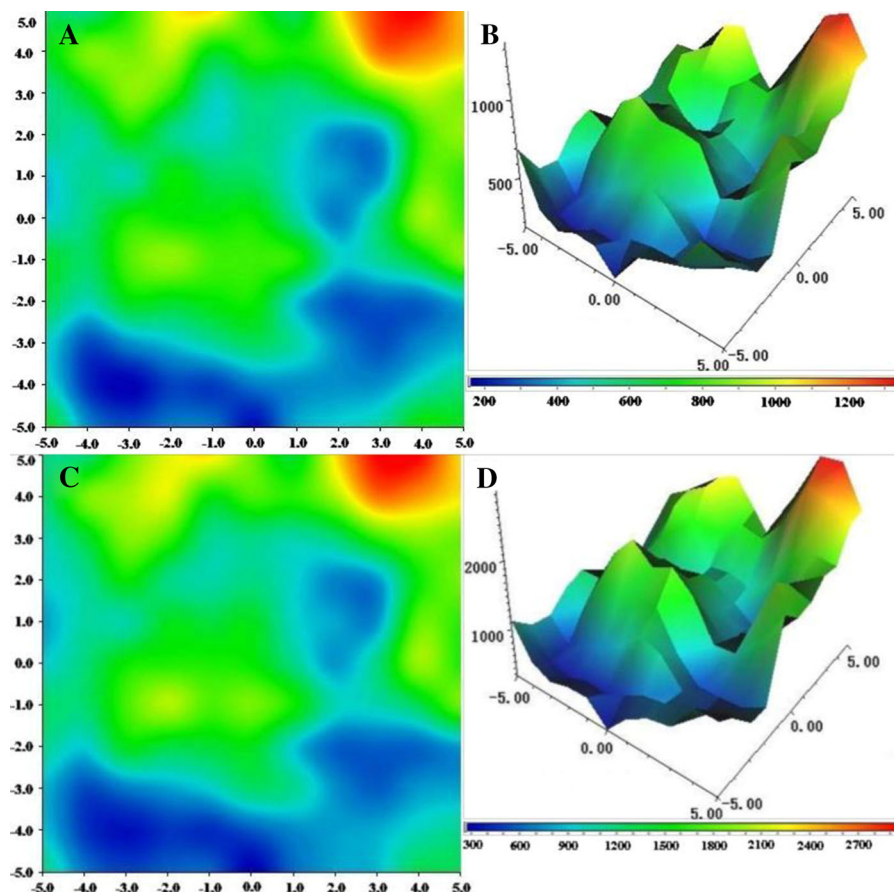

Fig. 6 Area scanning mapping of the Fe$_3$O$_4$/Ag (sputtering time 130 s) based on the intensity of the spectral peak at 1142 cm^{-1} (**A**, **B**) and 1437 cm^{-1} (**C**, **D**) of PATP. The range of the selected area is 5 cm $\times$ 5 cm
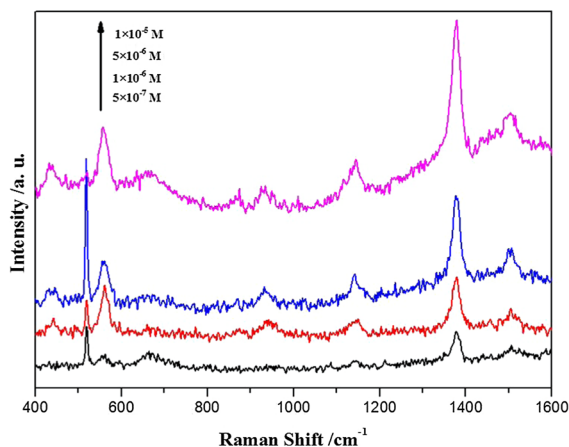
Fig. 7 SERS spectra of thiram with different concentrations from 1×10^{-5} M to 5×10^{-7} M adsorbed on the Fe_3O_4/Ag composites with the sputtering time of 130 s. The excitation power was 1.0 mW and the integration time was 5 s

2012; Rastegarzadeh et al. 2013; Queffelec et al. 2001; Waseem et al. 2010). However, these methods are complicated, time consuming or require expensive equipment. There were relatively small reports about the SERS detection of thiram. In our experiment, the Fe_3O_4/Ag composites were immersed into the thiram solution. Then, they were washed with ethanol and dried with high-purity nitrogen. Figure 7 shows the SERS spectra of thiram adsorbed on the Fe_3O_4/Ag composites with a sputtering time of 130 s. The main characteristic peaks of thiram were obtained. The strongest peak at 1379 cm^{-1} is attributed to the CN stretching mode and symmetric CH_3 deformation mode. The peak at 560 cm^{-1} is attributed to S–S stretching modes and those at 1145 and 1504 cm^{-1} to the CN stretching vibrations and rocking CH_3 mode, respectively (Tao et al. 2014; Kang et al. 2002). The concentration of thiram can be detected as low as 5×10^{-7} M (about 0.012 ppm), which is lower than the maximal residue limit of 7 ppm in fruit prescribed by the U.S. Environmental Protection Agency. In addition, the composites we prepared are convenient to carry, which can be potentially used for real-time detection of pesticides in the field.

Conclusions

In summary, the Fe_3O_4/Ag composites were obtained by magnetron sputtering technique. The SERS activity of the composites with different sputtering time was

detected with PATP and R6G as adsorbed molecules. The SERS intensity of the composites reached the maximum with the sputtering time of 130 s. As SERS substrate, the reproducibility and stability of the SERS signal is very well. Then this composite was used as an efficient SERS substrate for high-sensitivity detection of pesticide residues. The detection limits for thiram of the composites with a sputtering time of 130 s are as low as 5×10^{-7} M, which meets the requirements for ultratrace detection of analytes. We believe that these Fe_3O_4/Ag composites could serve as ideal substrates for SERS applications and provide an excellent candidate for SERS analysis.

References

Bao F, Li JF, Ren B, Yao JL, Gu RA, Tian ZQ (2008) Synthesis and characterization of Au@Co and Au@Ni core-shell nanoparticles and their applications in surface-enhanced Raman spectroscopy. J Phys Chem C 112(2):345–350

Bao F, Yao JL, Gu RA (2009) Synthesis of magnetic Fe_2O_3/Au core/shell nanoparticles for bioseparation and immunoassay based on surface-enhanced Raman spectroscopy. Langmuir 25(18):10782–10787

Bardhan R, Chen W, Torres CP, Bartels M, Huschka RM, Zhao LL, Morosan E, Pautler RG, Joshi A, Halas NJ (2009) Nanoshells with targeted simultaneous enhancement of magnetic and optical imaging and photothermal therapeutic response. Adv Funct Mater 19(24):3901–3909

Chen JY, Wang DL, Xi JF, Au L, Siekkinen A, Warsen A, Li ZY, Zhang H, Xia YN, Li XD (2007) Immuno gold nanocages with tailored optical properties for targeted photothermal destruction of cancer cells. Nano Lett 7(5):1318–1322

Gan ZB, Zhao AW, Zhang MF, Wang DP, Guo HY, Tao WY, Gao Q, Mao RR, Liu EH (2013) Fabrication and magnetic-induced aggregation of Fe_3O_4-noble metal composites for superior SERS performances. J Nanopart Res 15(11):1–124

Gao G, Wu H, Zhang Y, Luo T, Feng L, Huang P, He M, Cui D (2011) Synthesis of ultrasmall nucleotide-functionalized superparamagnetic gamma-Fe_2O_3 nanoparticles. CrystEngComm 13(15):4810–4813

Gao G, Wang K, Huang P, Zhang YX, Zhi X, Bao CC, Cui DX (2012) Superparamagnetic Fe_3O_4-Ag hybrid nanocrystals as a potential contrast agent for CT imaging. CrystEngComm 14(22):7556–7559

Gühlke M, Selve S, Kneipp J (2012) Magnetic separation and SERS observation of analyte molecules on bifunctional

silver/iron oxide composite nanostructures. J Raman Spectrosc 43(9):1204–1207

Guo HY, Ruan FX, Lu LH, Hu JW, Pan JG, Yang ZL, Ren B (2009a) Correlating the shape, surface plasmon resonance, and surface-enhanced Raman scattering of gold nanorods. J Phys Chem C 113(24):10459–10464

Guo SJ, Dong SJ, Wang EK (2009b) A general route to construct diverse multifunctional Fe_3O_4/metal hybrid nanostructures. Chem Eur J 15:2416–2424

Guo HY, Zhao AW, Gao Q, Li D, Zhang MF, Gan ZB, Wang DP, Tao WY, Chen XC (2014) One-step synthesis of Ag-Fe_3O_4 nanocomposites and their SERS properties. J Nanopart Res 16(8):2538

Gupta B, Rani M, Kumar R (2012) Degradation of thiram in water, soil and plants: a study by high-performance liquid chromatography. Biomed Chromatogr 26(1):69–75

Jiang WQ, Zhou YF, Zhang YL, Xuan SH, Gong XL (2012) Superparamagnetic $Ag@Fe_3O_4$ core-shell nanospheres: fabrication, characterization and application as reusable nanocatalysts. Dalton Trans 41(15):4594–4601

Jun BH, Kim G, Baek J, Kang H, Kin T, Hyeon T, Jeong DH, Lee YS (2011) Magnetic field induced aggregation of nanoparticles for sensitive molecular detection. Phys Chem Chem Phys 13(16):7298–7303

Kang JS, Hwang SY, Lee CJ, Lee MS (2002) SERS of dithio-carbamate pesticides adsorbed on silver surface; thiram. Bull Korean Chem Soc 23(11):1604–1610

Khosroshahi ME, Ghazanfari L (2012) Physicochemical characterization of Fe_3O_4/SiO_2/Au multilayer nanostructure. Mater Chem Phys 133(1):55–62

Lal S, Grady NK, Kundu J, Levin CS, Lassiter JB, Halas NJ (2008) Tailoring plasmonic substrates for surface enhanced spectroscopies. Chem Soc Rev 37(5):898–911

Lee SY, Hung L, Lang GS, Cornett JE, Mayergoyz ID, Rabin O (2010) Dispersion in the SERS enhancement with silver nanocube dimers. ACS Nano 4:5763–5772

Liu SP, Chen N, Li LX, Pang FF, Chen ZY, Wang TY (2013) Fabrication of Ag/Au core-shell nanowire as a SERS substrate. Opt Mater 35(3):690–692

Lv BL, Xu Y, Tian H, Wu D, Sun YH (2010) Synthesis of $Fe_3O_4\backslash SiO_2\backslash Ag$ nanoparticles and its application in surface-enhanced Raman scattering. J Solid State Chem 183(12):2968–2973

Mariotti D, Sankaran RM (2010) Microplasmas for nanomaterials synthesis. J Phys D Appl Phys 43(32):323001

Njoki PN, Lim IS, Mott D, Park HY, Khan B, Mishra S, Sujakumar R, Luo J, Zhong CJ (2007) Size correlation of optical and spectroscopic properties for gold nanoparticles. J Phys Chem C 111(40):14664–14669

Orendorff CJ, Gole A, Sau TK, Murphy CJ (2005) Surface-enhanced Raman spectroscopy of self-assembled mono-layers: sandwich architecture and nanoparticle shape dependence. Anal Chem 77(10):3261–3266

Osawa M, Matsuda N, Yoshii K, Uchida I (1994) Charge-transfer resonance Raman process in surface-enhanced Raman-scattering from *p*-aminothiophenol adsorbed on silver-herzberg-teller contribution. J Phys Chem 98(48):12702–12707

Pande S, Ghosh SK, Praharaj S, Panigrhi S, Basu S, Jana S, Pal A, Tsukuda T, Pal T (2007) Synthesis of normal and inverted gold-silver core-shell architectures in beta-cy-clodextrin and their applications in SERS. J Phys Chem C 111(29):10806–10813

Qi D, Zhang HY, Tang J, Deng CH, Zhang XM (2010) Facile synthesis of mercaptophenylboronic acid-functionalized core-shell structure $Fe_3O_4@C@$Au magnetic microspheres for selective enrichment of glycopeptides and glycoproteins. J Phys Chem C 114(20):9221–9226

Queffelec AL, Boisde F, Larue JP, Haelters JP, Corbel B, Thouvenot D, Nodet P (2001) Development of an immunoassay (ELISA) for the quantification of thiram in lettuce. J Agric Food Chem 49:1675–1680

Rastegarzadeh S, Pourreza N, Larki A (2013) Dispersive liquid–liquid microextraction of thiram followed by microvolume UV–Vis spectrophotometric determination. Spectrochim Acta Part A 114:46–50

Rodríguez-Fernández J, Funston AM, Pérez-Juste J, Álvarez-Puebla RA, Liz-Marzán LM, Mulvaney P (2009) The effect of surface roughness on the plasmonic response of individual sub-micron gold spheres. Phys Chem Chem Phys 11(28):5909–5914

Skrabalak SE, Au L, Li XD, Xia YN (2007) Facile synthesis of Ag nanocubes and Au nanocages. Nat Protoc 2(9):2182–2190

Su L, Jia WZ, Manuzzi DP, Zhang LC, Li XP, Gu ZY, Lei Y (2012) Highly sensitive surface-enhanced Raman scattering using vertically aligned silver nanopetals. RSC Adv 2(4):1439–1443

Sun LL, Song YH, Wang L, Guo CL, Sun YJ, Liu ZL, Li Z (2008) Ethanol-induced formation of silver nanoparticle aggregates for highly active SERS substrates and application in DNA detection. J Phys Chem C 112(5):1415–1422

Sun LJ, He J, An SS, Zhang JW, Ren D (2013) Facile one-step synthesis of $Ag@Fe_3O_4$ core-shell nanospheres for reproducible SERS substrates. J Mol Struct 1046:74–81

Tang XH, Dong RL, Yang LB, Liu JH (2015) Fabrication of Au nanorod-coated Fe_3O_4 microspheres as SERS substrate for pesticide analysis by near-infrared excitation. J Raman Spectrosc 46(5):470–475

Tao WY, Zhao AW, Sun HH, Gan ZB, Zhang MF, Li D, Guo HY (2014) Periodic silver nanodishes as sensitive and reproducible surface-enhanced Raman scattering substrates. RSC Adv 4(7):3487–3493

Tian Y, Chen LJ, Zhang J, Ma ZF, Song CN (2012) Bifunctional Au-nanorod@Fe_3O_4 nanocomposites: synthesis, characterization, and their use as bioprobes. J Nanopart Res 14(7):998

Wang JP, Yang L, Liu BH, Jiang HJ, Liu RY, Yang JW, Han GM, Mei QS, Zhang ZP (2014) Inkjet-printed silver nanoparticle paper detects airborne species from crystalline explosives and their ultratrace residues in open environment. Anal Chem 86(7):3338–3345

Waseem A, Yaqoob M, Nabi A (2010) Determination of thiram in natural waters using flow-injection with cerium(IV)–quinine chemiluminescence system. Luminescence 25(1):71–75

Xia XH, Zeng J, McDearmon B, Zheng YQ, Li QG, Xia YN (2011) Silver nanocrystals with concave surfaces and their

optical and surface-enhanced Raman scattering properties. Angew Chem Int Ed 50(52):12542–12546

Xu HX, Bjerneld EJ, Kall M, Borjesson L (1999) Spectroscopy of single hemoglobin molecules by surface enhanced Raman scattering. Phys Rev Lett 83(21):4357–4360

Xu CJ, Wang BD, Sun SH (2009) Dumbbell-like Au-Fe_3O_4 nanoparticles for target-specific platin delivery. J Am Chem Soc 131(12):4216–4217

Xuan SH, Zhou YF, Xu HJ, Jiang WQ, Leung KC, Gong XL (2011) One step method to encapsulate nanocatalysts within Fe_3O_4 nanoreactors. J Mater Chem 21(39):15398–15404

Yang LB, Bao ZY, Wu YC, Liu JH (2012) Clean and reproducible SERS substrates for high sensitive detection by solid phase synthesis and fabrication of Ag-coated Fe_3O_4 microspheres. J Raman Spectrosc 43(7):848–856

Yang J, Wang ZY, Zong SF, Chen H, Zhang RH, Cui YP (2014) Dual-mode tracking of tumor-cell-specific drug delivery using fluorescence and label-free SERS techniques. Biosens Bioelectron 51:82–89

Zhai YM, Zhai JF, Wang YL, Guo SJ, Ren W, Dong SJ (2009) Fabrication of iron oxide core/gold shell submicrometer spheres with nanoscale surface roughness for efficient surface-enhanced Raman scattering. J Phys Chem C 113(17):7009–7014

Zhang XP, Jiang WQ, Gong XL, Zhang Z (2010) Sonochemical synthesis and characterization of magnetic separable Fe_3O_4/Ag composites and its catalytic properties. J Alloys Compd 508(2):400–405

Zhang L, Luo Q, Zhang F, Zhang DM, Wang YS, Sun YL, Dong WF, Liu JQ, Huo QS, Sun HB (2012a) High-performance magnetic antimicrobial Janus nanorods decorated with Ag nanoparticles. J Mater Chem 22(45):23741–23744

Zhang YX, Ding HL, Liu YY, Pan SS, Luo YY, Li GH (2012b) Facile one-step synthesis of plasmonic/magnetic core/shell nanostructures and their multifunctionality. J Mater Chem 22(21):10779–10786

Zhang MF, Zhao AW, Li D, Sun HH, Wang DP, Guo HY, Gao Q, Gan ZB, Tao WY (2014) Generalized green synthesis of diverse LnF(3)-Ag hybrid architectures and their shape-dependent SERS performances. RSC Adv 4(18):9205–9212

Zong SF, Wang ZY, Yang J, Wang CL, Xu SH, Cui YP (2012) A SERS and fluorescence dual mode cancer cell targeting probe based on silica coated Au@Ag core-shell nanorods. Talanta 97:368–375